2024 IEEE/ASME International Conference on Advanced Intelligent Mechatronics (AIM)
July 15-19, 2024. Boston, MA, USA

Autonomous Motion Planning for a Motorized Walker Using Potential Field and Admittance Control

Gerardo Lopez, Mojtaba Sharifi, *Member, IEEE*,

***Abstract*— Assistive walkers are essential for many individuals who require geriatric care or mobility aids for day-to-day activities. The functionality of these devices is not able to provide the care that is needed for those with different levels of physical disabilities or who are visually or mentally impaired. Developing an autonomous powered walker that can receive a user's intent and assist them in navigating obstacles would allow more people to have access to enhanced mobility. In this work, a control strategy is designed for obstacle avoidance using potential field generation and admittance regulation. The mechatronics hardware and software are developed to generate and implement a continuous real-time motion trajectory for the smart walker in response to the user's interaction torque and scanned locations of obstacles in the environment. The integration of the mecanum wheels, DC motors, microcontrollers, a rotating LiDAR scanner, and a mini-PC powered by an onboard battery allowed for the evaluation and testing of the obstacle avoidance algorithm and admittance control in real time. The experimental results showed that the autonomous walker can generate desired trajectories in response to the user's interaction using the admittance controller and navigate around the obstacles with real-time velocity updates for the motorized wheels.**

I. Introduction

A. Community Need

Falls are extremely common and often go unreported with as many as a third of individuals over 65 falling once a year [1]. This group requires more attentive care and is expected to become a larger share of the population, creating a larger demand for mobility assistance [2]–[4]. The Centers for Disease and Control Prevention states that around 12.1% of adults in the US suffer from some form of disability affecting mobility [5]. This increased demand for mobility assistance will continue to put a strain on the healthcare professionals to assist the growing elderly population and other individuals with physical mobility impairments [6], [7]. Assistive devices are solutions to this need [8]–[11].

The type of assistive device is determined at the individual level by a trained medical professional and can range from wheelchairs, for those with extremely high assistance needs, to walkers and canes for those that require a lower level of assistance [12]. Although walkers help people with mobility issues get some independence back, it has been known that these devices are not 100% effective and can lead to serious injuries caused by falling [13]. Because of this, there has been considerable research focused on improvements to walkers in order to provide more personalized assistance for those who require it. These walkers have been called smart walkers because they significantly augment the walker's ability to safely assist the user in daily tasks, even for those with impaired cognitive and/or visual capacity [14]. The main design goals of these smart walkers are to improve the safety of traditional walkers by enhancing the user's postural stability and navigating their surroundings [15], [16].

Gerardo Lopez and Mojtaba Sharifi are with the Department of Mechanical Engineering, San Jose State University, CA, USA. (e-mail: gerardo.lopez@sjsu.edu, mojtaba.sharifi@sjsu.edu) *(Corresponding author: Mojtaba Sharifi)*

B. Types of Walkers

The use of impedance/admittance control for a smart walker has proven to be extremely beneficial in being able to reliably predict the user's intent. An advantage of force-based impedance-based controllers is the capability to determine the user's intention using a force-torque sensor. This requires that the force-torque sensor be placed in a location where all the interaction forces of the user are transmitted through the sensor to the walker's body [17]–[19]. The addition of sensors to prevent collision with objects in the environment can be performed by employing digital cameras, infrared, ultrasonic, or a combination of them. The main benefit of infrared and ultrasonic is that the data generated is easier to process since distance from the sensor is one of the captured parameters. A camera, on the other hand, is not able to provide distance readings as an output and needs to be further processed to determine objects in the walker's path. This data is then fed into the walker strategy to negotiate possible paths based on the user's intent [20], [21].

C. Collision Avoidance Strategies

The concept of potential field has been used for path planning in the fields of autonomous/semi-autonomous mobile robots and vehicles. This includes self-driving cars, unmanned aerial vehicles, autonomous ships, and tele-operated robots. In the case of a semi-autonomous system in which the desired trajectory is not predetermined by the system, the required inputs are the distance from the obstacle [22]. These control systems work by monitoring the distance between the object and the robot itself but only activate when the conditions of a possible collision occur. A collision avoidance strategy that has been employed in naval vessels is in the use of potential fields that can alter a ship's desired direction by any obstacle entering different zones of control [23]. These zones would be determined by the distance and ability of the vessel to navigate away from a possible collision. The avoidance algorithm won't be activated until the criteria for collision are met, which then would attempt to steer the vessel out of the collision path. The inclusion

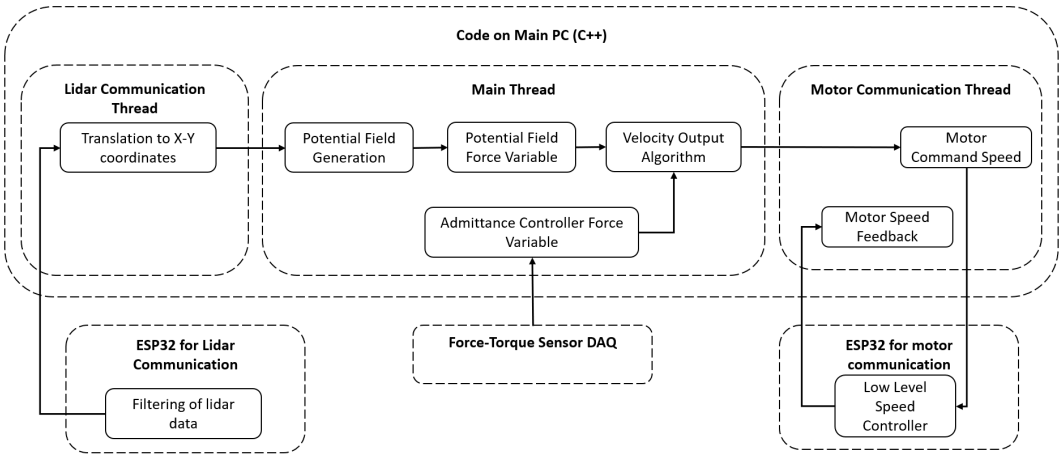

Fig. 1. Architecture of the developed mechatronic systems, the executed tasks, and signal transmission between different component (including a PC, microcontrollers, DC motors, force sensor, and LiDAR scanner)

of a negotiating zone, in addition to an emergency zone, for obstacle avoidance can assist the autonomous system in generating smoother responses to possible obstacles [24]. This method can also be extended to moving objects that enter the potential fields in which the object's speed can be determined.

The main goal of this work is to propose an intelligent control strategy and develop a mechatronic system to perform real-time motion planning for a motorized assistive walker based on the user and environment inputs. This trajectory shaping is conducted in response to the user's physical interaction and obstacle detection in space by integration of multiple sensors. A six-axis force-torque sensor is employed under the handlebar for the user's intention detection, a LiDAR sensor is used for scanning obstacles, and high-torque DC motors with motion feedback are utilized for all Mecanum wheels. An admittance controller is employed to generate the original motion (including the velocity direction and magnitude) in Cartesian space in terms of the user's physical interaction. By establishing different zones of control, the walker's avoidance algorithm can gently deliver the space feedback to the user by slowing (resisting) the movement in the direction of any obstacle within a specific range and increasing this resistance as the user gets closer to the obstacle. To this end, the potential fields are generated in real-time for scanned obstacles to regulate velocity modifications and update the motion trajectory using the proposed control scheme. This assistive walker will be helpful for the personalized locomotion of individuals with different levels of physical, visual, and mental impairments.

II. Design and Development of the Controls for the Assistive Walker

The mechatronic system development and components to implement the proposed control strategy are explained in this section. A rotating LiDAR sensor is utilized to observe the distance of objects around the walker to be used for the obstacle avoidance algorithm. A six-axis force-torque sensor is employed to measure the user's physical interaction in order to determine the user's intent (the desired direction and speed of motion). An admittance model is defined to generate the desired velocity vector in Cartesian space in terms of the measured interaction forces. This desired translation and rotational velocities are translated to the Mecanum wheels' space to be implemented by DC motors. Figure 1 shows the architecture of the developed mechatronic systems, the executed tasks, and signal transmission between different components. An ESP32 microcontroller is dedicated to the LiDAR communication process and the data (angle and distance) received from the RP LiDAR sensor and sent to the thread to be used in the main C++ code for motion planning. The communication thread converts the data into a matrix of x-y obstacle locations and stores it until requested by the main thread (C++ code). This main thread generates the potential field, determines user intent (velocity vector in Cartesian space, V_x and V_y) based on force-torque measurement, and computes the desired speed of the walker by converting the Cartesian speed into motors' rotation using a matrix transformation according to the kinematics of Macanum wheels. The corresponding equations for these components of the proposed motion planning strategy are mentioned in the next sections. An ESP32 microcontroller receives the speed vector of wheel rotations and converts it into individual CAN commands to the DC motors. The walker structure is shown in Fig. 2, which includes four omnidirectional wheels and DC motors, a force-torque sensor, LiDAR scanners, and a controller box that houses a mini PC, microcontrollers, a DAQ device, and a battery.

A. Mecanum Wheel Kinematics

Having a 4-wheeled vehicle with mecanum wheels, we can derive the forward and backward kinematics of this assistive walker [25]–[27]. In Eq. 1, a and b parameters are the distances of the wheels to the walker center in Cartesian x-y coordinates. w_i is the wheel speed while r is the radius of the wheels. w_z is the rotational speed of the walker around its z-axis, while v_x and v_y are the translational velocity components of the walker along the x

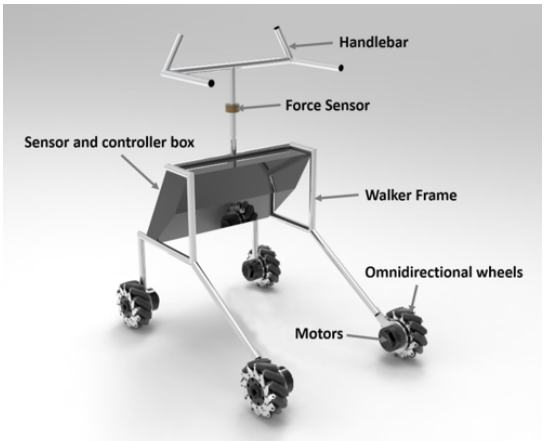

Fig. 2. Schematic of the smart walker with sensors, actuators, and controller box

and y axes, respectively. This kinematic equation is used for the generation of velocity commands to the DC motors in terms of the desired Cartesian speed of the walker.

$$\begin{bmatrix} w_1 \\ w_2 \\ w_3 \\ w_4 \end{bmatrix} = \frac{1}{r} \begin{bmatrix} 1 & -1 & -(a+b) \\ 1 & 1 & (a+b) \\ 1 & 1 & -(a+b) \\ 1 & -1 & (a+b) \end{bmatrix} \begin{bmatrix} v_x \\ v_y \\ w_z \end{bmatrix} \tag{1}$$

B. Obstacle Avoidance Development

For obstacle avoidance, the generation of the potential field zones is conducted for online modification of the movement trajectory when there is any object in a collision path with the walker. The variation of these zones also prevents the movement trajectory from changing drastically in different directions. These potential field zones created for the walker can be seen in Fig. 3. The size of the zone radius RZ where specified based on the walker's width w and D_{max} as the maximum distance traveled over the sampling rate dt.

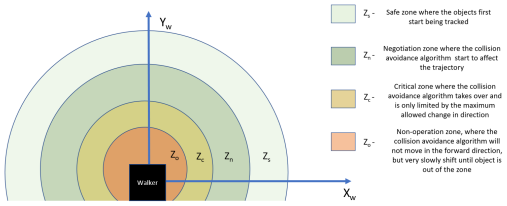

Fig. 3. Defined potential field zones for the autonomous assistive walker to perform stationary obstacle avoidance

$$\begin{bmatrix} RZ_0 \\ RZ_s \\ RZ_n \\ RZ_c \end{bmatrix} = \begin{bmatrix} D_{max}/dt + w \\ 5 \cdot RZ_0 \\ 2.5 \cdot RZ_0 \\ 1.5 \cdot RZ_0 \end{bmatrix} \tag{2}$$

The trajectory planning is limited by the maximum distance traveled between samples. The obstacle avoidance inside the negotiation zone is adjusted based on the walker's width and the potential field values defined in Eq. 3. The variable potential field value (PVF) is the magnitude of the potential field around the walker at a given distance. The direction value (DV) is positive or negative depending on the slope of the potential field, and v_{x_pf} and v_{y_pf} are the velocity outputs generated by the potential field.

$$\begin{bmatrix} v_{x_pf} \\ v_{y_pf} \end{bmatrix} = \begin{bmatrix} v_{y_max} \cdot \frac{PFV_{RZ_{measured}} - PFV_{RZ_n}}{PFV_{RZ_n} - PFV_{RZ_c}} \cdot DV \\ v_{x_max} \cdot \frac{PFV_{RZ_{measured}} - PFV_{RZ_n}}{PFV_{RZ_n} - PFV_{RZ_c}} \cdot DV \end{bmatrix} \tag{3}$$

The potential field generation is based on a heat map of the obstacles inside of RZ_s. This creates a parabolic repulsive field with a value of 1000 at the obstacle and a value of 0 at a distance of RZ_0 from the obstacle according to Eq. 4, where y and x range from 0 to RZ_n.

$$PotentialMatrix = 1000 - ((x^2 + y^2)/RZ_n^2) \cdot 1000 \tag{4}$$

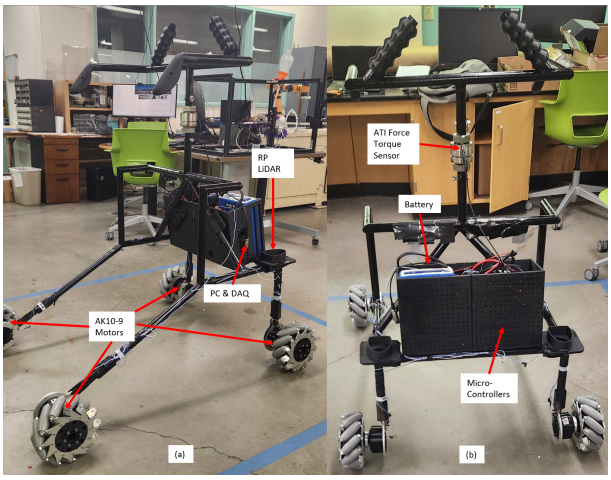

Fig. 4. Fully assembled walker: (a) Side view showing the locations of AK10-9 motors, mecanum wheels, RP LiDAR, and the DAQ and PC. (b) Front view showing the locations of microcontrollers, battery, and ATI force-torque sensor

C. Admittance Control

An admittance controller is developed and tested for the walker to generate the user's desired speed based on the interaction force and torque measured by the ATI sensor as shown in Fig. 4. The admittance control includes four variables including desired velocities in x and y directions, the rotational desired velocity, and the user balance variable. These translational and rotational velocities are determined by Eq. 5 in terms of the interaction torque or forces (T_i for $i = z$, x, or y). The inputs of this admittance model are the interaction torque in z direction for the axial rotation and the interaction forces in x and y directions for planar translation. The values of $T_{control}$ and T_{max} are determined experimentally for each user of the walker.

$$\begin{bmatrix} T_{low} < T_i < T_{high} : V_i = \frac{(T_i) abs(T_{high} - T_i)}{(T_{high})} \cdot V_{i_{max}} \\ T_{low} > T_i || T_i > T_{high} : V_i = 1 \\ abs(T_i) > T_{max} : V_i = 0 \end{bmatrix} \tag{5}$$

The user balance variable S_{user} is defined to determine user stability according to Eq. 6. For this balance, the force measurement in the z direction is used to determine the user's stability, in which the values beyond the low and

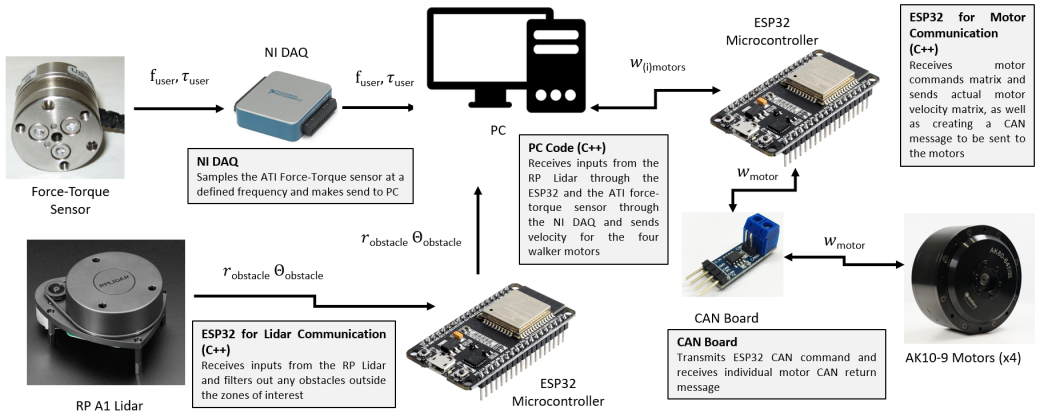

Fig. 5. Configuration of the mechatronic system for the smart walker with individual component outputs for the ATI force torque sensor, RP LiDAR, PC, ESP32 microcontrollers, and CAN board

high thresholds specify that the user is not being properly supported by the walker. The values for $S_{control_l}$, $S_{control_h}$, S_{min}, and S_{max} are determined experimentally for users based on their comfort and preference. The final desired velocity $V_{i_{final}}$ in Cartesian space is obtained using Eq. 7.

$$\begin{bmatrix} S_{min} < Fz_{user} < S_{control_l} : S_{user} = 1 + \frac{S_{control_l} - Fz_{user}}{S_{control_l} - S_{min}} \\ S_{control_l} < Fz_{user} < S_{control_h} : S_{user} = 1 \\ S_{control_h} < Fz_{user} < S_{max} : S_{user} = 1 + \frac{S_{max} - Fz_{user}}{S_{max} - S_{control_h}} \\ Fz_{user} > S_{high} || Fz_{user} < S_{min} : S_{user} = 0 \end{bmatrix} \tag{6}$$

$$V_{i_{final}} = V_i \cdot S_{user} \tag{7}$$

D. Hardware architecture

The fully integrated walker with mechatronic components is shown in Fig. 4. The microcontroller chosen for this system is ESP32 due to its ability to have multiple serial communications. The main PC and ESP32 communicate to the AK10-9 motors (from T-motors) by sending motor commands and receiving encoder feedback via the SN65HVD230 CAN board (from AITRIP). Another ESP32 board communicates via serial to receive information from the RP LiDAR 1A scanner (from SLAMTEC). The RP LiDAR has a rotation frequency of 10 Hz with a total of 1450 sample points per rotation. A 48V battery powers the whole mechatronic system with a power converter to step down the voltage for the PC and DAQ device (from National Instruments).

The components and configuration schematic of the walker's mechatronic system used to receive sensory information and control the motors are shown in Fig. 5. The software programming is conducted in C++ on the PC using Visual Studio Code due to its integration with PlatformIO IDE for the microcontrollers. The CAN messages required to control the AK10-9 motors and instructions for serial communication with the RP LiDAR sensor are explained in [28] and [29], respectively.

E. Software Architecture

The main C++ code is split into 3 threads to allow for processes of acquiring and sending data for the potential field generation and admittance controller calculations. The "Main

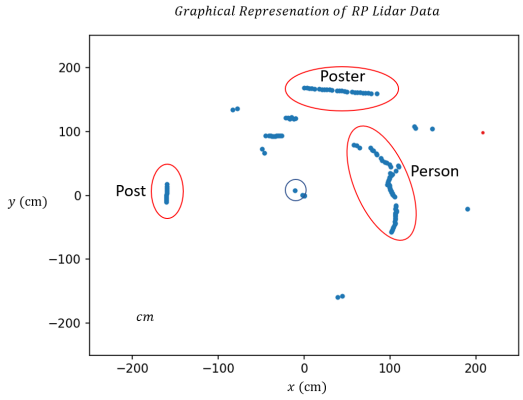

Fig. 6. Graphical representation of data received from the RP LiDAR sensor and processed to create a plot of obstacles around the sensor

Thread" has a computation time of 50ms due to the multiple matrix calculations needed to update the potential field matrix. The communication threads with other sensors and motors both have a sampling rate of 8 ms. The RP LiDAR delivers the angle and distance of all surfaces scanned by the rotating laser. This information is then transformed into the $x - y$ coordinate system considering the walker's front center as the origin. An experimental result of the processed data from the RP LiDAR is illustrated in Fig. 6 showing scanned obstacles around the sensor. The code uploaded on the ESP32 pre-filters the LiDAR data to ensure that only information that is required, which is the obstacle location within the RZ_s zone, is transmitted to the main PC code to reduce the data for serial communications.

The potential field generation portion of this code resets the obstacle distance matrix to accept updated values at the frequency of the main thread. The potential field generation is performed based on Eq. 4 to update the potential field matrix. Once the potential field matrix has been generated, Eq. 3 is employed to update the "Potential Field Force Variable" mentioned in Fig. 1. The "Velocity Output Algorithm" takes in the desired speed input from the user based on the admittance control and the "Potential Field Force Variable". The velocity variable is updated every time new values are generated by the potential field.

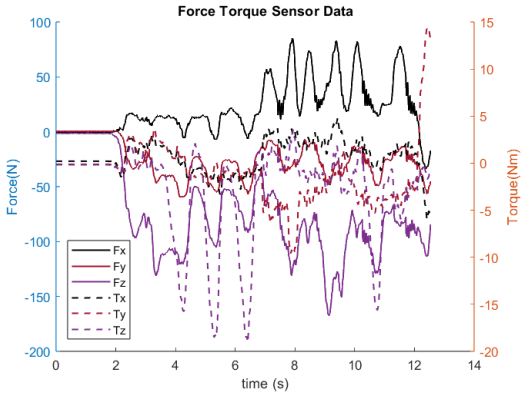

Fig. 7. Force and Torque measurement during the test of walker to determine the desired admittance-based velocity

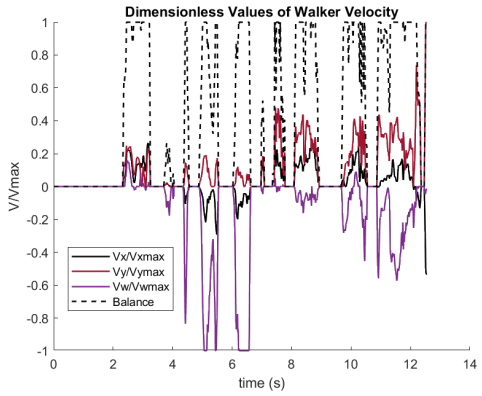

Fig. 8. Dimensionless desired velocity components of the walker based on the force and torque measurements illustrated in Fig. 7

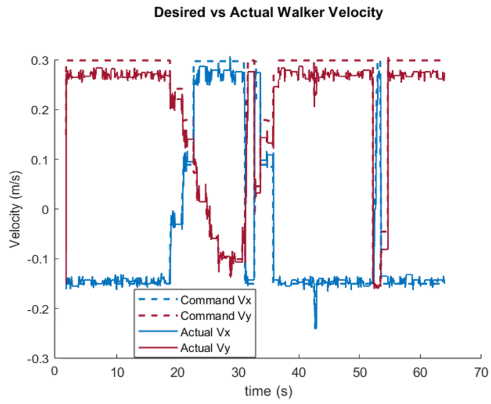

Fig. 9. Actual and desired velocities of the walker in x and y directions

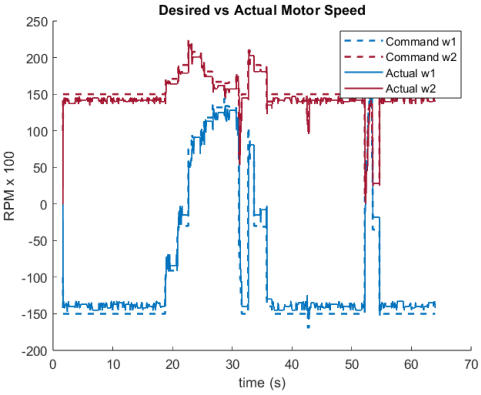

Fig. 10. Actual and desired speeds for two groups of the DC motors attached to the wheels

III. Experimental Evaluations

All components of the smart walker were integrated into a test bench first to conduct troubleshooting. The main experiments were conducted to evaluate the walker's performance in tracking desired velocities.

A. Admittance Control Experiments

In these experiments, a user attempted to move the walker in the desired direction as well as simulated instability. The following values were determined through various experiments based on a static walker; $S_{control_l}$ = -75 N, $S_{control_h}$ = -95 N, S_{min} = -60 N, S_{max} = -110 N, $T_{control}$ = 10 Nm and T_{max} = 30 Nm, which are used in Eqs. 5, 6 and 7 to determine the admittance-based desired velocity. Figure 7 shows the force and torque values measured by the ATI sensor under the handlebar. The obtained values for the desired velocity were processed and obtained as seen in Fig. 8. The user attempted to apply the torques T_x and T_y and the force F_z to move the walker. This is due to the geometry of the walker's handle and the user stability requirements resulting in lying down on both arms and guiding the walker by torques.

B. Obstacle Avoidance Experiments

With a constant desired velocity as the output of the admittance model, various tests were conducted in order to assess the performance of the potential field generation and the motor speed control. Figures 9, 10, 11 and 12 demonstrate the results of speed variation in Cartesian and wheels spaces, starting with an input velocity of 300 mm/s in the y direction. The speed controller's gain of the DC motor is adjusted on K_d = 3 and the sampling time of 10 ms is employed in these experiments. As shown in Fig. 11, the average errors between the desired and actual velocities are 20.2 mm/s in the y direction and 2.9 mm/s in the x direction. Figure 12 shows a graphical representation of the walker in Cartesian space and the performance of obstacle avoidance by online modification of the walker's speed as expected.

IV. Conclusion

In this study, an admittance control method and an obstacle avoidance strategy were developed and tested for a motorized assistive walker. For this purpose, the mechatronics hardware and software were developed to generate and execute a continuous real-time motion trajectory for the smart walker, responsive to both user interaction force and the spatial distribution of scanned obstacles. By integrating components such as mecanum wheels, DC motors, microcontrollers, a rotating LiDAR scanner, and a mini-PC powered by an onboard battery, the obstacle avoidance algorithm and admittance control strategy were implemented. Through experimental evaluations, the autonomous walker's capabilities are

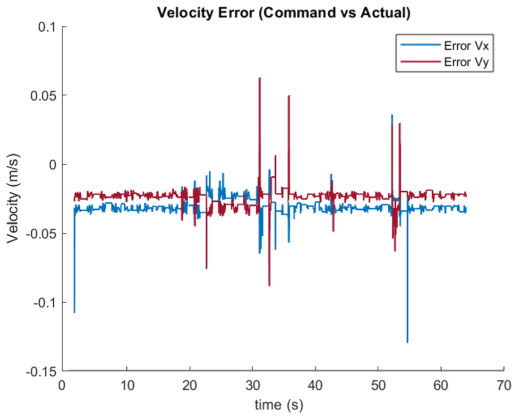

Fig. 11. Cartesian velocity errors in x and y directions for the walker as differences between actual and desired velocities

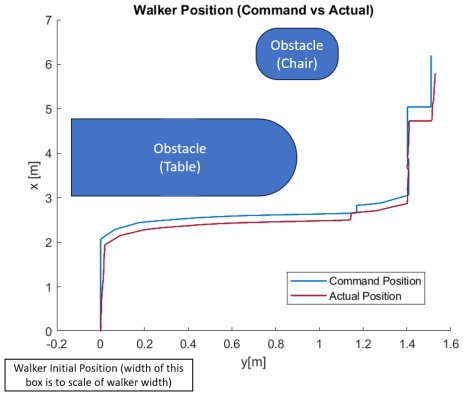

Fig. 12. Graphical representation of the smart walker's desired and actual position based on the actual and desired velocities (obstacles are approximately illustrated)

demonstrated in generating the desired velocity in response to the user's physical interaction, navigating surrounding obstacles, and real-time adjustment of the motion trajectory. In future work, online mapping of the environment using a depth camera and image processing can be integrated into the control system. Moreover, user studies will be conducted to assess the effectiveness of this smart walker in assisting people with disabilities and navigating different environments.

REFERENCES

[1] P. E. Tatum, S. Talebreza, and J. S. Ross, "The geriatric assessment: An office-based approach," *Am Fam Physician*, vol. 97, no. 12, pp. 776–784, 2018.

[2] M. M. Martins, C. P. Santos, A. F. Neto, and R. Ceres, "Assistive mobility devices focusing on smart walkers: Classification and review," *Robotics and Autonomous Systems*, vol. 60, no. 4, pp. 548–562, 2012.

[3] Q. Yan, J. Huang, C. Tao, X. Chen, and W. Xu, "Intelligent mobile walking-aids: perception, control and safety," *Advanced Robotics*, vol. 34, no. 1, pp. 2–18, 2020.

[4] U.S. Department of Commerce, "An aging nation: Projected number of children and older adults," *U.S. Census Bureau*, 2019.

[5] Center for Disease Control and Prevention, "Disability impacts all of us," *CDC*, 2023.

[6] J. Fong1, C. Martinez1, and M. Tavakoli, "Ways to learn a therapist's patient-specific intervention: Robotics- vs telerobotics-mediated hands-on teaching," *ICRA*, pp. 870–876, 2019.

[7] M. Oghogho, M. Sharifi, M. Vukadin, C. Chin, V. K. Mushahwar, and M. Tavakoli, "Deep reinforcement learning for emg-based control of assistance level in upper-limb exoskeletons," in *International Symposium on Medical Robotics (ISMR)*, 2022, pp. 1–7.

[8] D. M. Rivera and M. Sharifi, "Design and fabrication of a lightweight and wearable semirigid robotic knee chain exoskeleton," *ASME J of Medical Diagnostics*, vol. 7, no. 2, p. 021007, 2024.

[9] J. E. Patricio, M. Sharifi, D. Shrestha, S. H. S. Thu, and E. Kwan, "Design and development of a lightweight, high-torque, and cost-effective hip exoskeleton," in *IEEE/ASME International Conference on Advanced Intelligent Mechatronics (AIM)*, 2023, pp. 367–372.

[10] T. Cheng and M. Sharifi, "Development of an assistive ankle-foot exoskeleton with sensorized silicone-based insole," *ASME J of Medical Diagnostics*, vol. 7, no. 2, p. 021010, 2024.

[11] H. S. Mojtaba Sharifi, Saeed Behzadipour and M. Tavakoli, "Assist-as-needed policy for movement therapy using telerobotics-mediated therapist supervision," *Control Engineering Practice*, vol. 101, p. 104481, 2020.

[12] A. M. Eakman, M. D. Havens, S. J. Ager, R. L. Buchanan, N. J. Fee, S. G. Gollick, M. J. Michels, L. L. Olson, K. M. Satterfield, and K. A. Stevenson, "Fall prevention in long-term care: An in-house interdisciplinary team approach," *Geriatric Rehabilitation*, vol. 17, no. 3, pp. 29–39, 2002.

[13] B. H and M. BE, "Assistive devices for balance and mobility: Benefits, demands, and adverse consequences," *Archives of Physical Med and Rehabilitation*, vol. 86, no. 1, pp. 134–145, 2005.

[14] P. Viswanathan, E. P. Zambalde, G. Foley, J. L. Graham, R. H. Wang, B. Adhikari, A. K. Mackworth, A. Mihailidis, W. C. Miller, and I. M. Mitchell, "Intelligent wheelchair control strategies for older adults with cognitive impairment: user attitudes, needs, and preferences," *Autonomous Robots*, vol. 41, no. 3, pp. 539–554, 2016.

[15] M. Martins, C. Santos, A. Frizera, and R. Ceres, "A review of the functionalities of smart walkers," *Medical Engineering and Physics*, vol. 37, no. 10, pp. 917–928, 2015.

[16] S. McLachlan, J. Arblaster, O. Liu, J. Miro, and L. Chenoweth, "A multi-stage shared control method for an intelligent mobility assistant," *ICORR*, pp. 426–429, 2005.

[17] K. T. Song and S. Y. Jiang, "Force-cooperative guidance design of an omni-directional walking assistive robot," *IEEE*, 2011.

[18] C. Huang, "User's intent detection and shared control: Application to an intelligent walker," 2007.

[19] C. H. Ko, K. Y. Young, Y. C. Huang, and A. S. Kumar, "Active and passive control of walk-assist robot for outdoor guidance," *IEEE/ASME Transactions on Mechatronics*, vol. 18, no. 3, pp. 1211–1220, 2013.

[20] K. T. Song, S. Y. Jiang, and S. Y. Wu, "Safe guidance for a walking-assistant robot using gait estimation and obstacle avoidance," *IEEE/ASME Transactions on Mechatronics*, vol. 22, no. 5, pp. 2070–2078, 2017.

[21] D. Leite, M. Vellasco, and K. Figueiredo, "Robotic device for mobility assistance to elderly people in urban environments," 2016.

[22] Y. C. Liu and N. Chopra, "Control of semi-autonomous teleoperation system with time delays."

[23] H. Lyu and Y. Yin, "Colregs-constrained real-time path planning for autonomous ships using modified artificial potential fields," *The Journal of Navigation*, vol. 72, no. 3, pp. 588–608, 2019.

[24] Y. Chen, P. Wang, Z. Lin, and C. Sun, "Global path guided vehicle obstacle avoidance path planning with artificial potential field method," *Institution of Engineering and Technology*, vol. 5, no. 1, 2023.

[25] Z. Sun, H. Xie, J. Zheng, Z. Man, and D. He, "Path following control of mecanum wheels omnidirectional mobile robots using nonsingular terminal sliding mode," *Mechanical Systems and Signal Processing*, vol. 147, p. 107128, 2021.

[26] S. G. Racz, M. Crenganiș, R.-E. Breaz, A. Maroșan, A. Bârsan, C. E. Gîrjob, C. M. Biriș, and M. Tera, "Mobile robotsmdash;ahp-based actuation solution selection and comparison between mecanum wheel drive and differential drive with regard to dynamic loads," *Machines*, vol. 10, no. 10, 2022.

[27] H. Taheri, B. Qiao, and N. Ghaeminezhad, "Kinematic model of a four mecanum wheeled mobile robot," *International Journal of Computer Applications*, vol. 113, no. 3, pp. 6–9, 2015.

[28] [Online]. Available: https://store.tmotor.com/goods-1030-AK10-9.html

[29] [Online]. Available: https://www.slamtec.com/en/Support#rplidar-a-series